Improving antimicrobial therapy for Buruli ulcer

Omansen, Till Frederik

Chapter 5

In-vivo imaging of bioluminescent *Mycobacterium ulcerans:* a tool to refine the murine Buruli ulcer tail model

Manuscript accepted with Am J Trop Med Hyg 12/2018.

Till F. Omansen[1,2], Renee A. Marcsisin[1], Brendon Y. Chua[1], Weiguang Zeng[1], David C. Jackson[1], Jessica L. Porter[1], Ymkje Stienstra[2], Tjip S. van der Werf[2,3], Timothy P. Stinear[1]

[1] Department of Microbiology and Immunology, The Peter Doherty Institute for Infection and Immunity, University of Melbourne, Parkville, VIC 3010, Australia.
[2] University of Groningen, Department of Internal Medicine/Infectious diseases, University Medical Center Groningen, 9700 RB Groningen, The Netherlands.
[3] University of Groningen, Department of Pulmonary Diseases & Tuberculosis, University Medical Center Groningen, 9700 RB Groningen, The Netherlands.

ABSTRACT

Buruli ulcer is a neglected tropical disease caused by infection with *Mycobacterium ulcerans*. Unclear transmission, no available vaccine and sub-optimal treatment regimens hamper the control of this disease. Carefully designed, pre-clinical research is needed to address these shortcomings. In-vivo imaging (IVIS®) of infection is an emerging tool that permits monitoring of disease progression and reduces the need to using large numbers of mice at different time-points during the experiment, as individual mice can be imaged at multiple time-points. We aimed to further describe the use of (IVIS®) imaging in Buruli ulcer. We studied the detection of *M. ulcerans* in experimentally infected BALB/c mouse tails and the subsequent histopathology and immune response in this pilot study. IVIS®-monitoring was performed weekly in ten infected BALB/c mice to measure light emitted as a proxy for bacterial load. Nine out of ten (90%) BALB/c mice infected subcutaneously with $3.3x10^5$ *M. ulcerans* JKD8049 (containing pMV306 hsp16+luxG13) exhibited light emission from the site of infection indicating *M. ulcerans* growth *in-vivo*, while only five out of ten (50%) animals developed clinical signs of disease. Antibody titers were overall low and their onset was late. IFN- γ, and IL-10 were elevated in animals with pathology. Histopathology revealed clusters of acid-fast bacilli in the subcutaneous tissue, with macrophage infiltration and granuloma-formation resembling human Buruli ulcer. Our study successfully showed the utility of *M. ulcerans* IVIS® monitoring and lays a foundation for further research.

INTRODUCTION

Mycobacterium ulcerans causes the neglected tropical disease (NTD) Buruli ulcer (BU) that can manifest as skin nodule, plaque, edematous lesion or open skin ulcer characterized by yellowish-white necrosis and undermined edges (1). The disease generally occurs in clustered foci in rural Central and Western Africa but has also gained prominence in specific regions of south-east Australia. Currently, 12 countries actively report Buruli ulcer cases to the World Health Organization and 33 have ever reported cases (2). Patients with Buruli ulcer suffer from stigmatization, social participation restrictions and physical disability long after treatment is completed (3). The main pathogenic factor in BU is a diffusible cytotoxin called mycolactone. Mycolactone is a polyketide-derived macrolide that is responsible for the pathological triad of necrosis, suppressed local inflammatory response and hypoalgesia of the lesion (4,5). Mycolactone suppresses an efficient host innate and adaptive immune response by means of preventing protein translocation into the endoplasmic reticulum (6,7). The 174kb large plasmid pMUM001 is responsible for ML production by *M. ulcerans* (8).

There are several major challenges to control Buruli ulcer, such as uncertainty around the mode(s) of transmission, imperfect treatment regimens and the lack of a rapid diagnostic test. The mode of transmission is poorly understood and seems to vary by geographic location, although puncturing injuries after contamination from an environmental source seem to be at least one likely route of infection (9,10). In south-east Australia, mosquitoes have been linked to transmission (11,12). Buruli ulcer is currently treated with an eight-week regimen of rifampin and streptomycin or a regimen where the injectable streptomycin is replaced with clarithromycin after four weeks; a fully oral, eight-week rifampin and clarithromycin regimen has been trialed in humans and current trial analysis is ongoing (ClinicalTrials.gov Identifier: NCT01659437) (13,14). Progressed, larger lesions are often managed with antimicrobial treatment and, in addition, surgical excision of the infected tissue followed by functional repair and skin grafting (15); a recent study showed that the time-point for decision making on whether to intervene surgically or not does not matter for overall healing outcomes (16). No vaccine is available despite several efforts to employ the BCG-vaccine or to develop novel vaccines (17). Hence, more preclinical research in *M. ulcerans* transmission, chemotherapy and vaccination as well as pathogenesis, is necessary to solve the biomedical challenges complicating Buruli ulcer infection control.

M. ulcerans mouse-infection models have been pivotal in guiding research and clinical studies regarding these questions in the past (18-20). The mouse footpad and mouse tail infection are the two best established methods to study experimental infection with *M. ulcerans* in animals (18,21). The footpad-model has been derived from experience with experimental infection of *M. leprae* in mice (18,22). This model has been used in numer-

ous pre-clinical studies, to mainly evaluate drug efficacy, but also vaccines for *M. ulcerans* (19,20,23-35). Tail infection has been used to study pathology and vector research (21) and vaccinology (36). Given that Buruli ulcer is a subcutaneous infection mostly occurring on the lower and upper limbs in humans (1,37), the mouse footpad and tail are obvious sites to model the disease. The absence of fur in mice at these sites allows for easy clinical observation; a lower temperature of the skin on extremities compared to the core body, has also been hypothesized to favour the growth of *M. ulcerans*, which, in laboratory conditions grows best at 32°C. Tail infection offers a cutaneous infection site that is not in contact with the environment as much as the footpad so that contamination, re-distribution or loss of inoculum and animal impairment in more advanced stages of the disease are less likely to occur. Also, it is a more practical region for imaging than the footpad.

Pre-clinical studies such as drug efficacy and vaccine research need to assess the bacterial burden in lesions at given time-points. The method of choice for this is enumeration of colony-forming units (CFU) from mouse footpad homogenate; in order to obtain footpad samples, subsets of mice have to be culled at every time-point. The use of bioluminescence as read-out offers not only a reduction in sample size of such experiments but also allows us to refine the experiment because repeated measures can be taken non-invasively at many time-points in the same animal while CFUs are always compared to different mice which are biological replicate.

The use of bioluminescence represents a useful addition, or even alternative to CFU enumeration as its assessment can be carried out without killing the animal, allowing for serial testing in the same animal and reduction in overall sample size. Bioluminescent strains of *M. ulcerans* have been previously employed to evaluate drug efficacy in *in-vitro* and *in-vivo M. ulcerans* (30,31,35,38), as well as in vector ecology studies (10). Drug efficacy studies repurposed a luminometer for the read-out of bioluminescence, an apparatus designed to measure luminescence from bacteria in test vials. In this study, we sought to test a more advanced and sensitive read-out, namely an in-vivo imaging system (IVIS®) system for the imaging of bioluminescence from experimental murine *M. ulcerans* infection, all in the effort to further refine and reduce animal usage and aid the advance of much needed pre-clinical Buruli ulcer research. The Lumina XRMS Series III IVIS® camera used in this experiment has higher sensitivity compared to a luminometer. The IVIS® camera also allows overlaying of a photographic image with the detected light signal to visualize and localize bacteria, a luminometer only produces the quantification. We hypothesized that the application of modern IVIS® imaging technology allows us to thus sensitively detect bacteria when no outer clinical pathology is visible. An experimental low-burden infection with $3.3x10^5$ CFU *M. ulcerans* was selected, anticipating that some animals might not display visible pathology, to test the sensitivity of the IVIS camera. The bioluminescent *M. ulcerans* strain used in this study has

been previously described and contains the pMV306 hsp16+luxG13 reporter plasmid (38-40) that integrates into the mycobacterial chromosome and contains the lux operon (luxABCDE). Thus, it does not require the addition of an exogenous substrate to detect bioluminescence (39). Besides the demonstration of *M. ulcerans* imaging of early to advanced lesions, we also compared their histopathological appearance to reports of human cases. The immune response to our bioluminescent *M. ulcerans* strain was assessed to establish a baseline for further model development, and subsequent vaccine and transmission research.

MATERIALS AND METHODS

Culture conditions: *M. ulcerans* JKD8049 harbouring pMV306 hsp16+luxG13 was grown on Middlebrook 7H10 agar or in 7H9 broth containing 10% Oleic Albumin Dextrose Catalase Growth Supplement (Middlebrook, Becton Dickinson, Sparks, MD, USA), 0.5% glycerol and 25μg/ml kanamycin sulfate (Amresco, Solon, OH, USA). Plates and flasks were incubated for 8-10 weeks at 30°C, 5% CO_2. Liquid chromatography–mass spectrometry (LC-MS) was used to confirm that bioluminescent bacteria were still producing mycolactones (41).

Establishing a standard curve for bioluminescent *M. ulcerans* JKD8049: Light emission in photons/sec was compared with colony-forming units (CFU) for *M. ulcerans* JKD8049 cultured in Middlebrook 7H9 medium for 4 weeks and then diluted in serial 10-fold steps in 96-well trays. Photon emissions were captured using a Lumina XRMS Series III In Vitro Imaging System (IVIS®) (Perkin Elmer, Waltham, MA, USA). Bacterial CFUs were confirmed by the spot plate method (10).

Mouse-tail infections: Animal experimentation adhered to the Australian National Health and Medical Research Council Code for the Care and Use of Animals for Scientific Purposes and was approved by and performed in accordance with the University of Melbourne animal ethics committee (Application: 1312756.1). The animals were purchased from ARC (Canning Vale, Australia). Upon arrival, animals acclimatized for 5 days. Food and water were given *ad libitum*. Ten six-week old, female BALB/c mice were inoculated with approximately 10^5 *M. ulcerans* CFU by subcutaneous (SC) injection into the dorsal aspect of the upper third of the tail. The concentration of the bacterial inocula was confirmed by spot plating. After 17 weeks post-inoculation or whenever the humane endpoint was reached, mice were humanely killed.

***In-vivo* imaging:** Mice were imaged once a week during morning time using a Lumina XRMS Series III IVIS®. During imaging, mice were anaesthetized with 2.5% isofluorane gas (Ceva Animal Health, Glenorie, NSW, Australia). The stage on which the mice were placed during imaging was warmed to 37°C. Photon emissions were acquired with the following settings: exposure time 5 minutes, emission filter: open, excitation filter: blocked, binning: medium, F/stop 1. These images were superposed onto conventional black/white photographs (exposure time: auto, binning: medium, F/stop: 16). Images from the ventral and dorsal aspect of the tail were taken. Images were analyzed using Living Image® software. Areas emitting light were defined as regions of interest (ROI). A copy of every ROI was placed next to those areas for background measurement. Photons per second from the ROIs were computed and values from background regions subtracted from the actual ROI. Results from ventral and dorsal images (Fig. 1B) were added and the cumulative luminescence of the two imaging angles recorded.

ELISA: Blood samples were obtained by sub-mandibular puncture and, at experimental endpoint, by cardiac puncture. Serum was collected by centrifugation and stored at -20°C. All incubation of ELISA-plates was done in a moisturized container at room temperature. Flat-bottom polyvinyl chloride microtiter-plates (Thermo Fischer, Milford, MA, USA) were coated with 5μg of the antigen overnight. Antigens used were the mycobacterial small heat-shock protein 18 (Hsp18) and *M. ulcerans* whole cell lysate (WCL), prepared as previously described (42,43).The antigen was discarded and plates blocked for 1h with PBS containing 10mg/ml bovine serum albumin (BSA). Plates were washed four times with PBS containing 0.05% Tween-20 (PBST). Sera were added in eight serial dilutions in PBS to the plate and incubated for 4 h. Plates were washed with PBST again and 50μl/well HRP-conjugated polyclonal rabbit anti-mouse Ig-antibody (Dako, Glostrup, Denmark) was added in a 1:400 dilution in PBS for 1h. Subsequently, ELISA substrate (0.2 mM 2,29-azino-bis 3-ethylbenzthiazoline-sulfonic acid in 50 mM citric acid containing 0.004% hydrogen peroxide) was added to detect bound antibodies. Absorbance was read in a plate reader at 405nm and 450nm and the average of the two wavelengths recorded.

Intracellular cytokine staining and FACS: Dissected spleens were homogenized with a mesh (70μm cell strainer, Miltenyi Biotech (Germany) and ATC treated. Splenocytes ($1x10^6$) were re-stimulated with 2 μg *M. ulcerans* JKD8049 WCL in RPMI 1640 supplemented with 64 mM L-glutamine, 32 mM sodium pyruvate, 1.75 mM 2-mercaptoethanol, 3165 μg/ml penicillin (all Gibco® Life Technologies, NY, USA), 760 μg/ml gentamicin (G-Bioscience, St. Louis, MO, USA) and 10% heat-inactivated fetal calf serum (CSL, Parkville, Australia) for 72h at 37°C, 5% CO_2. Sixty-nine-well, round bottom plates, (Corning, NY, USA) were spun down, supernatant

collected and stored at -20°C. Cytokines were stained using the bead-based Cytometric Bead Array (CBA) Mouse Th1/Th2/Th17 Cytokine Kit (BD, North Ryde, NSW, Australia) according to the manufacturer's instructions. Samples were run on a BD FACSCanto™ II Flow Cytometry System and data analyzed using FCAP Array™ Analysis Software version 3.0.

Histology: A section ranging approximately 5mm from the midline of the ulcer proximally was dissected and stored in 10% buffered formalin for histological assessment. Prepared paraffin blocks were surface-decalcified with 10% nitric acid for 5 minutes before cutting 4µm sections. Hematoxylin and eosin (H&E) and Ziehl-Neelsen (ZN) staining were used following standard protocols. The specimens were subjected for analysis by an independent pathologist, who was blinded to the clinical extent of BU as well as to the BL results to reduce bias. Presence of AFB, inflammatory cells (macrophages, plasma cells/lymphocytes, neutrophils and eosinophils) as well as the degree of inflammation (granulomas, panniculitis, calcification, vasculitis, neuritis) and the tissue damage (dermal and fat tissue necrosis, muscle layer involvement and bone change) and the vascular involvement were scored. Specimens from two non-infected, naïve mice were used as controls.

Statistical analysis: Statistical analysis was performed using GraphPad Prism version 7.0a (GraphPad Software, Inc., San Diego, CA). Bioluminescence data were plotted as arithmetic mean of the ventral and dorsal reading, as described above. Time to bioluminescence is displayed as survival curve. Antibody titers are represented as the reciprocal of the highest dilutions of serum needed to measure an absorbance value of 0.2. This was achieved by transformation of the data by plotting absorbance values vs log0.5—fold dilutions data of each group and using a nonlinear regression analysis of to obtain a line of best fit (with 95% CI) to which the intersect value of 0.2 was determined. One-way ANOVA followed by a Tukey's multiple comparisons test assuming an alpha of 0.05 was used to test for statistical significant difference between antibody titer measurements. Cytokine readings are shown compared using descriptive statistics.

RESULTS

Standard curve comparing photon/s with CFU readout

To compare bioluminescence read-out with actual bacterial burden, we first established a standard curve *in-vitro*. We were able to interpolate a standard curve by nonlinear regression showing a very high positive correlation ($r^2 = 0.98$) between photons/s and CFU/ml (Fig 1A).

Establishment of mouse tail infection.

In order to evaluate virulence and to study murine infection, bioluminescent *M. ulcerans* was injected subcutaneously into mouse tails. The tail infection resulted in 90% (9 out of 10) of mice presenting measurable light emission on IVIS®-images. Other than at the injection site at the tail, no other foci of infection as indicated by bioluminescence were observed (Fig 1B). Fifty percent (5 out of 10) gradually developed macroscopically apparent lesions resembling Buruli ulcer within 17 weeks (Fig 1C). None of the animals showed other signs of illness than skin lesion that were restricted to the approximate sites of injection.

Course of the infection as measured by bioluminescence

To study the course of the infection in terms of bacterial burden measured in bioluminescence, mice were imaged weekly with the IVIS® system. Bioluminescence, measured in emitted photons/s rose exponentially to a maximum of $1x10^7$ in week seven (Fig 1D). Compared to our in-vitro generated standard curve, this would equal to approximately $5x10^6$ CFU/ml (Fig 1A) and was associated with advanced, severe pathology (Table 1). From this time-point on, the signal declined to a $1x10^5$ (corresponding to $4x10^4$ bacteria on the in-vitro standard curve) threshold until the end of the experiment. At week eight, three mice reached the humane endpoint and were euthanized. In examining the antibody titer levels against MU WCL, these began to rise in week 8, co-occurring with a decrease in photon/s counts. Animals displaying severe symptoms (swelling, redness and impeding ulceration, scabbing of the tail) had higher photons/s counts, indicating higher bacterial burden, compared to those with moderate (redness and minor swelling) or no pathology. Photons/sec counts increased per week until week 6-8 when the infection seemed to plateau.

Antibody titers

To characterize the antibody-mediated immune response to *M. ulcerans*, we obtained plasma samples for ELISA at weeks 2, 4, 8, 13 and 17 of the experiment. Over time, there was a slight increase of antibody titers in response to *M. ulcerans* WCL but overall a late onset of the antibody response was noted (Fig 2A). Antibody titers reached higher levels between week 11 and 17, but overall titers, were low (Fig 2A). The response to *M. ulcerans* Hsp18 and WCL was compared and no statistically significant difference ($p > 0.05$) was found (Fig 2B). Furthermore, ELISA results in response to WCL at week 8 were compared between animals with severe, moderate and no clinical pathology and no statistically significant difference ($p > 0.05$) was found (Fig 2C,D).

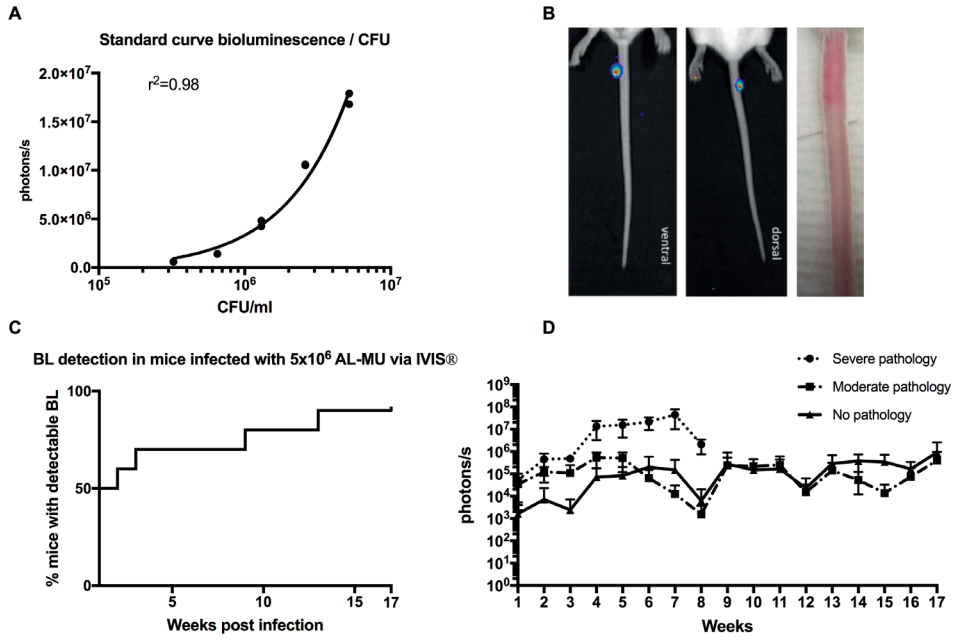

Figure 1. Use of bioluminescent *M. ulcerans* to follow the evolution of disease in the mouse tail model of Buruli ulcer. (A) Standard curve comparing bioluminescence and colony-forming units (CFU) of the *M. ulcerans* JKD8049 +pMV306 hsp16 luxG13 reporter strain. (B) IVIS®- (left) and photographic images (right) from BALB/c mice infected via subcutaneous tail inoculation with approx. $3.3x10^5$ CFU/ml *M. ulcerans* harboring the bioluminescent reporter plasmid. Photons/s emitted from bioluminescent bacteria were detected by IVIS® in anesthetized mice. Results are represented in a pseudo-colored scheme (red indicated high, yellow medium and green low intensity of light emitted). Light was detected from both the dorsal (site of injection) and ventral aspects of the mouse tail. The photos were taken at 4 weeks post infection; the bioluminescence read-out was $1.8x10^6$ photons, corresponding to approx. $6.7x10^5$ CFU/ml according to our standard curve. (C) Survival-graph representing time to detectable bioluminescence emission from mice infected with bioluminescent *M. ulcerans* into the tail (D) Development of mean photons/s emitted from mice infected with $3.3x10^5$ bioluminescent *M. ulcerans* into the upper third of the dorsal tail. Values represent the mean of dorsal and ventral photons/s measurement. Animals were sub-grouped for analysis by clinical staging based on severity of the gross pathology (*severe*: redness, swelling, edema, impending ulceration; *moderate*: redness, edema; and no pathology.

Late suppression of cytokines

To characterize and study the cytokine profile in our murine *M. ulcerans* infection model, intracellular cytokine staining was performed on spleen samples after eight and 17 weeks of the experiment, when three and seven mice were humanely killed, respectively. The cytokine concentrations in splenocyte samples re-stimulated with 2µg *M. ulcerans* JKD8049 WCL were compared between mice with pathology culled at week 8 and those with and without pathology culled at week 17. In the three mice that were culled prematurely due

to rapidly extending disease in week 8, elevated levels of IFN-γ and IL-10 were measured. Overall, cytokine levels were very low for all assayed cytokines in week 17 regardless of clinical state of the animal (Fig 3).

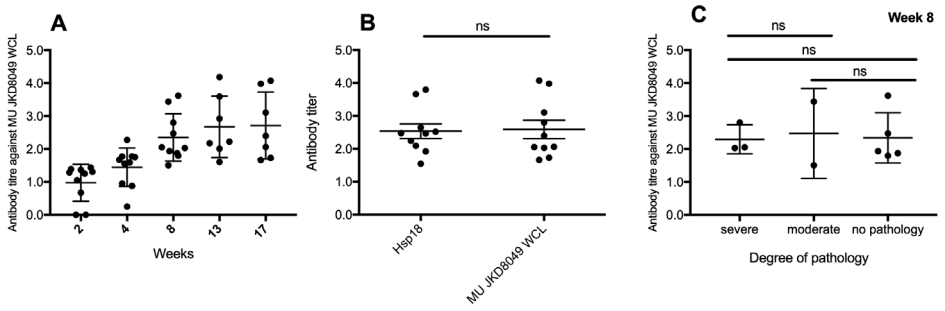

Figure 2. Evolution of the antibody titer against *M. ulcerans* whole cell lysate (WCL) and small heat shock protein 18 (Hsp18) measured in plasma from mice infected with *M. ulcerans* over time. A late onset of overall antibody response against an unspecific *M. ulcerans* whole cell lysate was noted in the bioluminescent *M. ulcerans* tail infection model. Antibody titers rose late, after 8 weeks and plateaued at week 13 (A). No difference ($p > 0.5$) was observed in the antibody titer against small heat-shock protein 18 (Hsp 18) and whole cell lysate (B). No statistically significance in antibody levels was seen between animals with severe, moderate or no apparent pathology ($p > 0.5$; C).

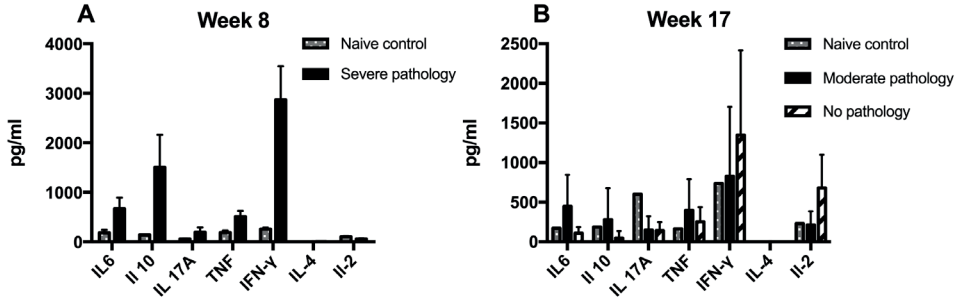

Figure 3: Comparison of cytokine profile assessed by intracellular cytokine staining (ICS) of mice infected with bioluminescent *M. ulcerans* after 8 (A) and 17 (B) weeks of infection to naïve, non-infected mice. Error bars represent standard error of the mean. Mice with advanced clinical pathology sacrificed at week eight of the experiment displayed highly elevated IFN-γ, as well as IL-6 and IL-10 levels (A). IFN-γ is known to activate macrophages and is a key regulator in granuloma formation in mycobacterial infections. At week 17, infected mice with no apparent pathology had higher IFN-γ counts than other mice, as well as slightly elevated IL-2 levels.

Histopathology of lesions

In order to validate the model and study the pathology of *M. ulcerans,* histopathology was performed on skin lesions and compared to those of humans described in the literature (44,45). Specimens from infected tissue were subjected to histopathological analysis in Ziehl-Neelsen and H&E-staining. Aggregates of acid-fast bacilli, *M. ulcerans*, were observed

at 300 – 400 µm beneath the epidermis (Fig 4A). Furthermore, epidermal hyperplasia and immune cell infiltrates were apparent (Fig. 4). Bioluminescence (photons/s) as proxy for bacterial quantity correlated well with the histological extent of disease except for mouse ID 87 (Table 1). Numerous acid-fast bacilli as well as severe, multifocal, chronic inflammation marked by presence of plasma cells, macrophages and lymphocytes were observed in mice with severe clinical pathology. There was extensive tissue damage, as well as vascular involvement in these animals. Mice with moderate clinical pathology exhibited mild and rather diffuse histological pictures and less tissue damage. Mice that had no obvious clinical signs of disease had low bioluminescence and showed moderate to little localized/focal histological features of inflammation (Table 1, Fig 4).

Table 1: Overview of histopathological findings of mice subcutaneously infected with autoluminescent *M. ulcerans* into the tail. Animals were divided by clinical pathology in severe pathology, moderate pathology and no marcopathology. Photons per second analyzed by IVIS®-imaging are shown in comparison to histological results. The amount of photos/s as a proxy for bacterial quantity correlated with pathology except in mouse 87, where no clinical pathology was seen.

Clinical picture	ID	BL-AUC	AFB	INF	TDM	VAS	Inflammatory cell type	Degree of inflammation
Severe pathology (sacrificed at week 8)	84	1.36E+08	++	+++	+++	n/a	PC, MΦ, LYM	Severe, multifocal, chronic
	85	1.35E+08	+++	+++	+++	n/a	PC, MΦ, LYM, EOS	Severe, multifocal, chronic
	88	1.72E+07	++	+++	+++	++	PC, MΦ, LYM	Severe, multifocal, chronic
Moderate pathology	86	1.97E+06	-	+	+	+	MΦ, LYM	Mild to moderate, chronic, multifocal
	89	3.69E+06	+	+/++	++	++	PC, MΦ	Mild, diffuse, chronic
No macro pathology	81	2.15E+06	-	+	+	-	MΦ, LYM	Moderate, chronic, focal
	82	692641	-	-	-	-	-	None
	83	872438	-	+	+	+	MΦ, LYM	Moderate, chronic, multifocal
	87	7.24E+06	++	+++	+++	++	PC, MΦ, LYM	Locally severe, chronic
	90	0	-	+	+	+	PC, MΦ, EOS, NEU	Mild, chronic, multifocal

ID, Identifier; BL-AUC, Bioluminescence in photons/s Area under the Curve; AFB, acid-fast bacilli, INF, inflammation; TDM, tissue damage; VAS, vascular involvement; PC, Plasma cell; MΦ, Macrophage, LYM, lymphocyte; EOS, eosinophil; NEU, neutrophil.

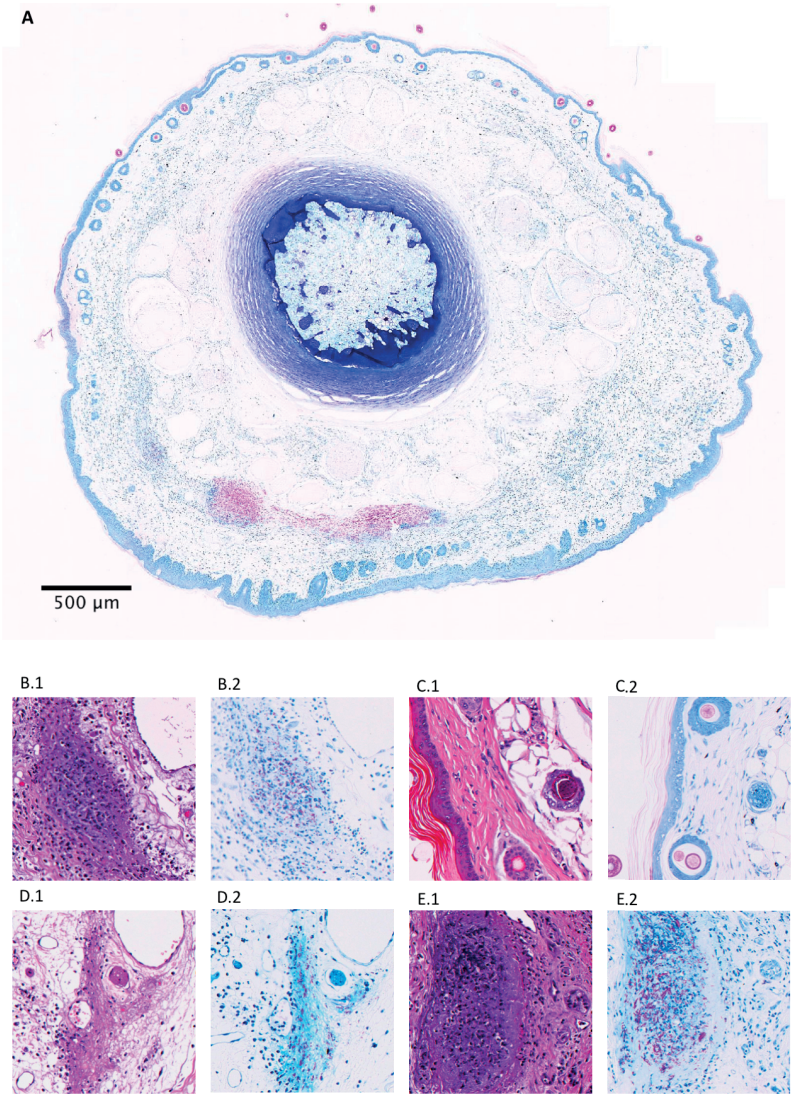

Figure 4: Histological specimens of mice infected with *M. ulcerans* into the tail in Hematoxylin and Eosin (H&E; A1,B1,C1,D1) or Ziel-Neelsen (ZN; A2,B2, C2,D2) staining. (A) Whole slide cross-section of mouse tail (ID #85) infected with *M. ulcerans* subcutaneously, humanely killed eight weeks' post-infection due to advanced clinical pathology. Visible, are clusters of acid-fast bacilli and in the cutis and subcutis, approx. 300-400 µm beneath the surface. (B.1 and B.2) Example of presence of AFB in mouse # 85, as well as granuloma formation. (C.1 and C2.) Normal mouse tail histology of a naïve, uninfected mouse with thin epidermis and intact hair follicles. (D.1 and D.2) Moderate pathology (mouse #89) with diffuse inflammation, tissue damage and presence of AFB. Involvement of blood vessels with zones of inflammation and also destruction of smaller vessels was visible in this specimen, too (vasculopathy). (E1,E2) Necrosis, granuloma formation, inflammation and abundant extracellular clustering of AFB was observed in mice with severe pathology (mouse #84).

DISCUSSION

In this study, we have successfully shown the applicability of IVIS® imaging of *Mycobacterium ulcerans* in a low-burden experimental subcutaneous tail infection mouse model. The lesion histopathology correlated with previously reported human pathology. The use of bioluminescent *M. ulcerans* JKD8049 (pMV306 hsp16+luxG13) allowed the infection to be followed and characterization of host immune responses to *M. ulcerans* in BALB/c mice. The onset of clinical signs was gradual and mice developed characteristic, localized lesions. Necrosis of the subcutis, chronic inflammation with the presence of macrophages and lymphocytes, granuloma formation, panniculitis, as well as the presence of AFBs correlating with disease progression are hallmarks of Buruli ulcer histopathology described in humans (46,47). The extent of and the overall pathology observed in the mouse tail tissue in our study was comparable to the above-mentioned experience from human patients supporting the use of this mouse model to study Buruli ulcer (44,45).

The bioluminescent read-out correlated with the histopathological outcome in a dose-dependent manner, where an elevated photons/s counts, indicating high bacterial burden coincided with more progressive histological disease (Table 1) underlining the usefulness of IVIS®-imaging and bioluminescence as a marker for disease progression. Both clinically apparent and non-apparent lesions could be visualized with IVIS® highlighting its sensitivity and usefulness in imaging early or low-burden infection. The use of bioluminescent *M. ulcerans* permitted us also to verify the location of the bacteria; after subcutaneous injection we observed presence of photon-emission exclusively in the upper-third of the mouse tail, which was the site of injection. This underlines the concept of BU as a localized infection, where disease manifestations only occur at the site of inoculation.

We approximated the growth rate in the lesion by comparison to an *in vitro*-derived standard curve. We noticed a decline and plateauing of bioluminescence from week 8 onwards. This phenomenon could be explained by a plateauing of the bacterial growth curve in the lesion and transition into a stationary phase where less of the immunosuppressive toxin mycolactone is produced and partial host control is established. This latter conclusion is supported to some extent by the rise of antibody titers around that time-point, also decreased transcription of the bioluminescence plasmid and hence decreased luminescence could be an issue interfering with light emission (Fig 2). Vasculopathy is a feature of Buruli ulcers observed in humans (46) and mice (Table 1, Fig 4). A hypoxic state within the lesion might also decrease bioluminescence and more research is needed to elucidate the usefulness of bioluminescence as a marker of bacterial quantity beyond approx. 8 weeks of infection in the BALB/c mouse. Overall, IVIS® imaging of *Mycobacterium ulcerans* had been applied in one study prior to this where it was used as a read-out in transmission research examining

different routes of infection, e.g. mosquito bite or needle stick trauma (10). In this pilot study, we developed this idea further and tested IVIS® imaging of experimentally infected mice with the aim to refine the mouse tail model of Buruli ulcer and to create a baseline knowledge of host immune response to the autoluminescent strain for subsequent vaccine studies.

Immunology and course of disease

The immune response to *M. ulcerans* is influenced by the microbes' toxin, mycolactone. Dendritic cells (DC's) are inhibited by ML which can impair their ability to prime cellular immune responses and phagocytose the bacteria (48). Also, suppression of a CD4+ immune response was observed in humans (49,50) and efficient mounting of a Th1 response and elevated IFN-γ seemed protective (51). T-cells-depletion, mediated by miRNAs has also been attributed to ML (52). It is believed that, like in tuberculosis, an effective cell-mediated immune response can naturally control the infection and is likely also important for conferring transient protection against BU, experimentally (53). Markedly elevated cytokines in human Buruli cases are IFN-γ and IL-10 (54). IFN-γ is known to be an early mediator of host response to *M. ulcerans* (55) and increases in patients after 4 – 8 weeks of antimicrobial treatment indicating immunocompetence against *M. ulcerans* and the mounting of a supportive CD4+ Th1-response (54). The elevated IFN-γ response seen in mice with severe pathology (Fig 3A) can thus be interpreted as an early reaction to a large amount of actively multiplying bacteria, whereas at week 17, mice with no pathology had higher IFN-γ levels than those with pathology possibly due to sufficient host control of the pathogen. Consistently, patients with pre-ulcerative lesions (early-phase) and patients with healed lesions (host control) both showed elevated IFN-γ levels (56) whilst IL-10 seems to be somewhat nonspecifically elevated during all phases of Buruli ulcer disease (51,54,56).

In our experiment, we noted a late onset of cell-mediated immunity in the mice infected with *M. ulcerans.* Antibody titers slowly rose, but only at week 8. The decline in photons/s and the increase in antibody titers coincided in week 7-8. It is not clear if rising antibody levels helped to gain control of the infection or if declining bacterial load resulted in less immune suppression by ML and led to a reactivation of the immune system and an increase of antibody levels. In humans, serological screening for Hsp18 antibodies indicates that large parts of the population in endemic areas are exposed to *M. ulcerans* but only some develop the disease (57). Guinea pigs infected with *M. ulcerans* appear to self-heal as do some mice (58). Furthermore, spontaneous loss of the plasmid encoding for the PKS-synthases that produce the *M. ulcerans* toxin mycolactone has been observed in mice. In that case *M. ulcerans* was rendered non-pathogenic (59). It is conceivable that humans infected with certain doses of *M. ulcerans* develop either no disease, limited disease, or even unnoticed

disease that self-resolves. Evidence for these scenarios has been observed in Buruli ulcer patients who have defaulted from antibiotic treatment regimens, yet could still be contacted for follow-up and showed to have healed lesions despite incomplete treatment (60). It is likely, that the bacterial burden was not zero in these patients at the time of default but that it reached a critical nadir at which host immunity overcame the counteracting effect of mycolactone and controlled infection. Individuals that are able to establish an efficient immune response to MU might control and clear the infection unnoticed as was the case with 50% of subcutaneously infected mice in our experiment. We have previously deduced a low infectious dose 50% (ID50) of <10 CFU from experiments involving mechanical injury simulated by needle stick to *M. ulcerans* externally contaminated mouse tails (10). Even though in this current research, bacterial presence was measured by IVIS® imaging in 90% of mice, only 50% of animals showed clinical disease in this experiment following subcutaneous injection with approx. $3.3x10^6$ CFU/ml. This observation and discrepancy with our previous research might be explained by the different handling of the inoculating needle, perpendicular, and supposedly deeper penetration in the study by Wallace et al. (10) and more superficial penetration in a 20-30° angle in subcutaneous injections in this study. Experiments are required to assess the *M. ulcerans* ID50 using carefully controlled inoculation conditions, perhaps using a micromanipulator with decreasing doses of *M. ulcerans*.

At week 8, three of the infected animals of the had reached the humane experimental endpoint and were culled. Their cytokine profile data were comparable to those of the other animals culled at week 17 and provide an insight into the evolution of the cytokine profile. While there were considerable amounts of IFN-γ and IL-10 indicating a Th1-mediated response observed in the animals sacrificed at week 8, all cytokine levels were reduced by week 17. The suppression of cytokines is due to inhibition by ML of nascent membrane and secretory proteins egress through the ER membrane (6,61). In human patients with Buruli ulcer, overall suppressed IFN-γ levels are seen (51). The triad of peak bacterial load with worsening pathology, low but rising antibody titers and elevated Th1 subset cytokines in week 7 could also explain the paradoxical response seen in patients; an overreaction and inflammation of the reactivating immune system noted in patients beginning antibiotics for Buruli ulcer (62). Animals not showing clinical signs of disease had marginally higher antibodies levels against *M. ulcerans* (Fig 2) possibly indicating some sort of immune response to the infection, though the results were statistically not significant in our small sample.

We demonstrated virulence of the *M. ulcerans*+pMV306 hsp16+luxG13 reporter strain and observed localized clinical disease with human-like pathology in 50% of the animals after inoculation with $3.3x10^6$ CFU/ml bacteria. There are several limitations to our study. We did not assess CFU counts in the lesions at the disease endpoint; processing of tail sections for histopathology instead in order to compare histopathology of the bioluminescent

strain was prioritized in this early, proof-of-principle study. Previous studies have shown a good correlation between CFU and luminescence in the mouse footpad model, at least for the first 8 weeks of the disease (31,35). Future studies should re-confirm this relationship with IVIS® imaging in a larger experiment. Furthermore, technical inconsistencies, especially while injecting the bacteria into the fine skin of the BALB/c mouse, can also account for different results. The immune parameters measured are in line with previous finding in the literature, as described above but are also derived form a small sample-size in this experiment. They should therefore be understood as a baseline for further studies rather than a basis for the discussion of Buruli ulcer pathology.

We successfully applied IVIS®-imaging of the bioluminescent *M. ulcerans* JKD8049 (pMV306 hsp16+luxG13) to the murine tail-infection model. We hope that the tool presented here will be used in future research on *M. ulcerans* and aid in pre-clinical research. We strongly believe that the application of modern, non-invasive in-vivo bacterial imaging can reduce and refine animal experimentation in Buruli ulcer research. We will continue to test and validate this model and apply it for the study of Buruli ulcer transmission and vaccination research.

Acknowledgements

We thank Rolfe Howlett and John Hayman and for help with analyzing and scoring the histopathological results.

REFERENCES

1. van der Werf TS, Stienstra Y, Johnson RC, Phillips R, Adjei O, Fleischer B, et al. Mycobacterium ulcerans disease. Bull World Health Organ. 2005 Oct;83(10):785–91.
2. WHO. Buruli ulcer. Factsheet. 16 April 2018. Consulted 20 November 2018. Available at: https://www.who.int/news-room/fact-sheets/detail/buruli-ulcer-(mycobacterium-ulcerans-infection)
3. de Zeeuw J, Omansen TF, Douwstra M, Barogui YT, Agossadou C, Sopoh GE, et al. Persisting social participation restrictions among former Buruli ulcer patients in Ghana and Benin. Small PLC, editor. PLoS Negl Trop Dis. Public Library of Science; 2014 Nov;8(11):e3303.
4. George KM, Chatterjee D, Gunawardana G, Welty D, Hayman J, Lee R, et al. Mycolactone: a polyketide toxin from Mycobacterium ulcerans required for virulence. Science. 1999 Feb 5;283(5403):854–7.
5. George KM, Pascopella L, Welty DM, Small PL. A Mycobacterium ulcerans toxin, mycolactone, causes apoptosis in guinea pig ulcers and tissue culture cells. Infect Immun. 2000 Feb;68(2):877–83.
6. Hall BS, Hill K, McKenna M, Ogbechi J, High S, Willis AE, et al. The pathogenic mechanism of the Mycobacterium ulcerans virulence factor, mycolactone, depends on blockade of protein translocation into the ER. Deretic V, editor. PLoS Pathog. 2014 Apr;10(4):e1004061.
7. Demangel C, High S. Sec61 blockade by mycolactone: a central mechanism in Buruli ulcer disease. Biol Cell. 2018 Jul 28.
8. Stinear TP, Mve-Obiang A, Small PLC, Frigui W, Pryor MJ, Brosch R, et al. Giant plasmid-encoded polyketide synthases produce the macrolide toxin of Mycobacterium ulcerans. Proc Natl Acad Sci USA. 2004 Feb 3;101(5):1345–9.
9. Meyers WM, Shelly WM, Connor DH. Heat treatment of Mycobacterium ulcerans infections without surgical excision. Am J Trop Med Hyg. 1974 Sep;23(5):924–9.
10. Wallace JR, Mangas KM, Porter JL, Marcsisin R, Pidot SJ, Howden B, et al. Mycobacterium ulcerans low infectious dose and mechanical transmission support insect bites and puncturing injuries in the spread of Buruli ulcer. Azman AS, editor. PLoS Negl Trop Dis. 2017 Apr;11(4):e0005553.
11. Johnson PDR, Azuolas J, Lavender CJ, Wishart E, Stinear TP, Hayman JA, et al. Mycobacterium ulcerans in mosquitoes captured during outbreak of Buruli ulcer, southeastern Australia. Emerging Infect Dis. 2007 Nov;13(11):1653–60.
12. Lavender CJ, Fyfe JAM, Azuolas J, Brown K, Evans RN, Ray LR, et al. Risk of Buruli ulcer and detection of Mycobacterium ulcerans in mosquitoes in southeastern Australia. Raoult D, editor. PLoS Negl Trop Dis. 2011 Sep;5(9):e1305.
13. Etuaful S, Carbonnelle B, Grosset J, Lucas S, Horsfield C, Phillips R, et al. Efficacy of the combination rifampin-streptomycin in preventing growth of Mycobacterium ulcerans in early lesions of Buruli ulcer in humans. Antimicrob Agents Chemother. American Society for Microbiology; 2005 Aug;49(8):3182–6.
14. Nienhuis WA, Stienstra Y, Thompson WA, Awuah PC, Abass KM, Tuah W, et al. Antimicrobial treatment for early, limited Mycobacterium ulcerans infection: a randomised controlled trial. Lancet. 2010 Feb 20;375(9715):664–72.
15. Kibadi K, Boelaert M, Fraga AG, Kayinua M, Longatto-Filho A, Minuku J-B, et al. Response to treatment in a prospective cohort of patients with large ulcerated lesions suspected to be Buruli Ulcer (Mycobacterium ulcerans disease). Phillips RO, editor. PLoS Negl Trop Dis. 2010 Jul 6;4(7):e736.
16. Wadagni AC, Barogui YT, Johnson RC, Sopoh GE, Affolabi D, van der Werf TS, et al. Delayed versus standard assessment for excision surgery in patients with Buruli ulcer in Benin: a randomised controlled trial. Lancet Infect Dis. 2018 Jun;18(6):650–6.

17. Einarsdottir T, Huygen K. Buruli ulcer. Hum Vaccin. 2011 Nov;7(11):1198–203.
18. Dega H, Robert J, Bonnafous P, Jarlier V, Grosset J. Activities of several antimicrobials against Mycobacterium ulcerans infection in mice. Antimicrob Agents Chemother. American Society for Microbiology (ASM); 2000 Sep;44(9):2367–72.
19. Bentoucha A, Robert J, Dega H, Lounis N, Jarlier V, Grosset J. Activities of new macrolides and fluoroquinolones against Mycobacterium ulcerans infection in mice. Antimicrob Agents Chemother. American Society for Microbiology; 2001 Nov;45(11):3109–12.
20. Dega H, Bentoucha A, Robert J, Jarlier V, Grosset J. Bactericidal activity of rifampin-amikacin against Mycobacterium ulcerans in mice. Antimicrob Agents Chemother. American Society for Microbiology (ASM); 2002 Oct;46(10):3193–6.
21. Marsollier L, Robert R, Aubry J, Saint André J-P, Kouakou H, Legras P, et al. Aquatic insects as a vector for Mycobacterium ulcerans. Appl Environ Microbiol. 2002 Sep;68(9):4623–8.
22. Shepard CC. The experimental disease that follows the injection of human leprosy bacilli into foot-pads of mice. J Exp Med. 1960 Sep 1;112(3):445–54.
23. Tanghe A, Dangy J-P, Pluschke G, Huygen K. Improved protective efficacy of a species-specific DNA vaccine encoding mycolyl-transferase Ag85A from Mycobacterium ulcerans by homologous protein boosting. Small PLC, editor. PLoS Negl Trop Dis. 2008 Mar 19;2(3):e199.
24. Tanghe A, Adnet P-Y, Gartner T, Huygen K. A booster vaccination with Mycobacterium bovis BCG does not increase the protective effect of the vaccine against experimental Mycobacterium ulcerans infection in mice. Infect Immun. 2007 May;75(5):2642–4.
25. Dhople AM, Namba K. Activities of sitafloxacin (DU-6859a), either singly or in combination with rifampin, against Mycobacterium ulcerans infection in mice. J Chemother. 2003 Feb;15(1):47–52.
26. Converse PJ, Almeida DV, Tasneen R, Saini V, Tyagi S, Ammerman NC, et al. Shorter-course treatment for Mycobacterium ulcerans disease with high-dose rifamycins and clofazimine in a mouse model of Buruli ulcer. Small PLC, editor. PLoS Negl Trop Dis. 2018 Aug 13;12(8):e0006728.
27. Converse PJ, Xing Y, Kim KH, Tyagi S, Li S-Y, Almeida DV, et al. Accelerated detection of mycolactone production and response to antibiotic treatment in a mouse model of Mycobacterium ulcerans disease. Phillips RO, editor. PLoS Negl Trop Dis. 2014;8(1):e2618.
28. Sarfo FS, Converse PJ, Almeida DV, Zhang J, Robinson C, Wansbrough-Jones M, et al. Microbiological, histological, immunological, and toxin response to antibiotic treatment in the mouse model of Mycobacterium ulcerans disease. Small PLC, editor. PLoS Negl Trop Dis. 2013;7(3):e2101.
29. Converse PJ, Almeida DV, Nuermberger EL, Grosset JH. BCG-mediated protection against Mycobacterium ulcerans infection in the mouse. Roy CR, editor. PLoS Negl Trop Dis. 2011 Mar 15;5(3):e985.
30. Zhang T, Li S-Y, Converse PJ, Almeida DV, Grosset JH, Nuermberger EL. Using bioluminescence to monitor treatment response in real time in mice with Mycobacterium ulcerans infection. Antimicrob Agents Chemother. 2011 Jan;55(1):56–61.
31. Zhang T, Bishai WR, Grosset JH, Nuermberger EL. Rapid assessment of antibacterial activity against Mycobacterium ulcerans by using recombinant luminescent strains. Antimicrob Agents Chemother. 2010 Jul;54(7):2806–13.
32. Almeida D, Converse PJ, Ahmad Z, Dooley KE, Nuermberger EL, Grosset JH. Activities of rifampin, Rifapentine and clarithromycin alone and in combination against mycobacterium ulcerans disease in mice. Diemert DJ, editor. PLoS Negl Trop Dis. 2011 Jan 4;5(1):e933.

33. Almeida DV, Converse PJ, Li S-Y, Tyagi S, Nuermberger EL, Grosset JH. Bactericidal activity does not predict sterilizing activity: the case of rifapentine in the murine model of Mycobacterium ulcerans disease. Johnson C, editor. PLoS Negl Trop Dis. 2013;7(2):e2085.
34. Converse PJ, Tyagi S, Xing Y, Li S-Y, Kishi Y, Adamson J, et al. Efficacy of Rifampin Plus Clofazimine in a Murine Model of Mycobacterium ulcerans Disease. Phillips RO, editor. PLoS Negl Trop Dis. 2015;9(6):e0003823.
35. Zhang T, Li S-Y, Converse PJ, Grosset JH, Nuermberger EL. Rapid, serial, non-invasive assessment of drug efficacy in mice with autoluminescent Mycobacterium ulcerans infection. Ricaldi JN, editor. PLoS Negl Trop Dis. 2013;7(12):e2598.
36. Coutanceau E, Legras P, Marsollier L, Reysset G, Cole ST, Demangel C. Immunogenicity of Mycobacterium ulcerans Hsp65 and protective efficacy of a Mycobacterium leprae Hsp65-based DNA vaccine against Buruli ulcer. Microbes Infect. 2006 Jul;8(8):2075–81.
37. Yerramilli A, Tay EL, Stewardson AJ, Kelley PG, Bishop E, Jenkin GA, et al. The location of Australian Buruli ulcer lesions-Implications for unravelling disease transmission. Pluschke G, editor. PLoS Negl Trop Dis. 2017 Aug;11(8):e0005800.
38. Omansen TF, Porter JL, Johnson PDR, van der Werf TS, Stienstra Y, Stinear TP. In-vitro activity of avermectins against Mycobacterium ulcerans. Johnson C, editor. PLoS Negl Trop Dis. Public Library of Science; 2015 Mar;9(3):e0003549.
39. Andreu N, Zelmer A, Fletcher T, Elkington PT, Ward TH, Ripoll J, et al. Optimisation of bioluminescent reporters for use with mycobacteria. Doherty TM, editor. PLoS ONE. 2010 May 24;5(5):e10777.
40. Andreu N, Zelmer A, Sampson SL, Ikeh M, Bancroft GJ, Schaible UE, et al. Rapid in vivo assessment of drug efficacy against Mycobacterium tuberculosis using an improved firefly luciferase. J Antimicrob Chemother. 2013 Sep;68(9):2118–27.
41. Hong H, Gates PJ, Staunton J, Stinear T, Cole ST, Leadlay PF, et al. Identification using LC-MSn of co-metabolites in the biosynthesis of the polyketide toxin mycolactone by a clinical isolate of Mycobacterium ulcerans. Chem Commun (Camb). 2003 Nov 21;(22):2822–3.
42. Gooding TM, Johnson PD, Campbell DE, Hayman JA, Hartland EL, Kemp AS, et al. Immune response to infection with Mycobacterium ulcerans. Infect Immun. 2001 Mar;69(3):1704–7.
43. Pidot SJ, Porter JL, Marsollier L, Chauty A, Migot-Nabias F, Badaut C, et al. Serological evaluation of Mycobacterium ulcerans antigens identified by comparative genomics. Phillips RO, editor. PLoS Negl Trop Dis. 2010 Nov 2;4(11):e872.
44. Mwanatambwe M, Fukunishi Y, Yajima M, Suzuki K, Asiedu K, Etuafel S, et al. Clinico-histopathological findings of Buruli ulcer. Nihon Hansenbyo Gakkai Zasshi. 2000 Jul;69(2):93–100.
45. Ruf M-T, Schütte D, Chauffour A, Jarlier V, Ji B, Pluschke G. Chemotherapy-associated changes of histopathological features of Mycobacterium ulcerans lesions in a Buruli ulcer mouse model. Antimicrob Agents Chemother. 2012 Feb;56(2):687–96.
46. Guarner J, Bartlett J, Whitney EAS, Raghunathan PL, Stienstra Y, Asamoa K, et al. Histopathologic features of Mycobacterium ulcerans infection. Emerging Infect Dis. 2003 Jun;9(6):651–6.
47. Rondini S, Horsfield C, Mensah-Quainoo E, Junghanss T, Lucas S, Pluschke G. Contiguous spread of Mycobacterium ulcerans in Buruli ulcer lesions analysed by histopathology and real-time PCR quantification of mycobacterial DNA. J Pathol. 2006 Jan;208(1):119–28.
48. Coutanceau E, Decalf J, Martino A, Babon A, Winter N, Cole ST, et al. Selective suppression of dendritic cell functions by Mycobacterium ulcerans toxin mycolactone. J Exp Med. 2007 Jun 11;204(6):1395–403.

49. Phillips R, Sarfo FS, Guenin-Macé L, Decalf J, Wansbrough-Jones M, Albert ML, et al. Immunosuppressive signature of cutaneous Mycobacterium ulcerans infection in the peripheral blood of patients with buruli ulcer disease. J Infect Dis. 2009 Dec 1;200(11):1675–84.
50. Boulkroun S, Guenin-Macé L, Thoulouze M-I, Monot M, Merckx A, Langsley G, et al. Mycolactone suppresses T cell responsiveness by altering both early signaling and posttranslational events. J Immunol. 2010 Feb 1;184(3):1436–44.
51. Gooding TM, Johnson PDR, Smith M, Kemp AS, Robins-Browne RM. Cytokine profiles of patients infected with Mycobacterium ulcerans and unaffected household contacts. Infect Immun. 2002 Oct;70(10):5562–7.
52. Guenin-Macé L, Carrette F, Asperti-Boursin F, Le Bon A, Caleechurn L, Di Bartolo V, et al. Mycolactone impairs T cell homing by suppressing microRNA control of L-selectin expression. Proc Natl Acad Sci USA. 2011 Aug 2;108(31):12833–8.
53. Fraga AG, Martins TG, Torrado E, Huygen K, Portaels F, Silva MT, et al. Cellular immunity confers transient protection in experimental Buruli ulcer following BCG or mycolactone-negative Mycobacterium ulcerans vaccination. Manganelli R, editor. PLoS ONE. 2012;7(3):e33406.
54. Sarfo FS, Phillips RO, Ampadu E, Sarpong F, Adentwe E, Wansbrough-Jones M. Dynamics of the cytokine response to Mycobacterium ulcerans during antibiotic treatment for M. ulcerans disease (Buruli ulcer) in humans. Clin Vaccine Immunol. 2009 Jan;16(1):61–5.
55. Bieri R, Bolz M, Ruf M-T, Pluschke G. Interferon-γ Is a Crucial Activator of Early Host Immune Defense against Mycobacterium ulcerans Infection in Mice. Johnson C, editor. PLoS Negl Trop Dis. 2016 Feb;10(2):e0004450.
56. Schipper HS, Rutgers B, Huitema MG, Etuaful SN, Westenbrink BD, Limburg PC, et al. Systemic and local interferon-gamma production following Mycobacterium ulcerans infection. Clin Exp Immunol. 2007 Dec;150(3):451–9.
57. Diaz D, Döbeli H, Yeboah-Manu D, Mensah-Quainoo E, Friedlein A, Soder N, et al. Use of the immunodominant 18-kiloDalton small heat shock protein as a serological marker for exposure to Mycobacterium ulcerans. Clin Vaccine Immunol. 2006 Dec;13(12):1314–21.
58. Silva-Gomes R, Marcq E, Trigo G, Gonçalves CM, Longatto-Filho A, Castro AG, et al. Spontaneous Healing of Mycobacterium ulcerans Lesions in the Guinea Pig Model. Johnson C, editor. PLoS Negl Trop Dis. 2015 Dec;9(12):e0004265.
59. Nakanaga K, Ogura Y, Toyoda A, Yoshida M, Fukano H, Fujiwara N, et al. Naturally occurring a loss of a giant plasmid from Mycobacterium ulcerans subsp. shinshuense makes it non-pathogenic. Sci Rep. 2018 May 29;8(1):8218.
60. Klis S, Kingma RA, Tuah W, van der Werf TS, Stienstra Y. Clinical outcomes of Ghanaian Buruli ulcer patients who defaulted from antimicrobial therapy. Trop Med Int Health. 2016 Sep;21(9):1191–6.
61. Simmonds RE, Lali FV, Smallie T, Small PLC, Foxwell BM. Mycolactone inhibits monocyte cytokine production by a posttranscriptional mechanism. J Immunol. 2009 Feb 15;182(4):2194–202.
62. Nienhuis WA, Stienstra Y, Abass KM, Tuah W, Thompson WA, Awuah PC, et al. Paradoxical responses after start of antimicrobial treatment in Mycobacterium ulcerans infection. Clin Infect Dis. 2012 Feb 15;54(4):519–26.